




# Vibration suppression of a geometrically nonlinear beam with boundary inertial nonlinear energy sinks

Zhen Zhang · Zhi-Tong Gao · Bo Fang · Ye-Wei Zhang 

Received: 26 July 2021 / Accepted: 26 April 2022 / Published online: 8 May 2022  
© The Author(s), under exclusive licence to Springer Nature B.V. 2022

**Abstract** As a simplified model of structures of many kinds, the Euler Bernoulli beam has proved useful for studying vibration suppression. In order to meet engineering design requirements, inertial nonlinear energy sinks (I-NESs) can be installed on the boundaries of an elastic beam to suppress its vibration. The geometric nonlinearity of the elastic beam is here considered. Based on Hamilton's principle, the dynamic governing equations of an elastic beam are established. The steady-state response of nonlinear vibration is obtained by the harmonic balance method and verified by numerical calculation. It is found that the geometric nonlinearity of the beam principally affects the first-order main resonance and reduces the response amplitude. An uncoupled system and the coupled I-NES system both show strong nonlinear hardening characteristics. I-NES achieves good vibration suppression. Finally, the optimal range of parameters for different damping is discussed. The results show that the vibration reduction effect of an optimized inertial nonlinear energy sink can reach 90%.

**Keywords** Inertial nonlinear energy sink · Geometric nonlinearity · Steady-state response · Vibration reduction

## 1 Introduction

The Euler Bernoulli beam is a simplified model for many structures in practical applications, such as aerospace, shipbuilding, and the automobile industry, where vibration can lead to structural damage. Studying the suppression of vibration in Euler Bernoulli beams is therefore important. Vibration control by a nonlinear energy sink (NES) has attracted more and more attention and much in-depth research in many countries. The frequency bandwidth of NES is significantly greater than that of the traditional linear vibration damper [1]. In NES, the energy transfer caused by vibration is unidirectional and irreversible [2, 3]. Viguié et al. calculated the nonlinear normal modes of the two-degree-of-freedom nonlinear system coupled with an NES by numerical continuation method, and analyzed the mechanism of energy transfer and dissipation. In this paper, the underlying Hamiltonian system is first considered [4]. Then, the transient passive control of nonlinear primary system with an NES is first exhaustive studied, and a qualitative tuning methodology is developed [5]. Gourc et al. coupled NES into LO oscillator, analyzed the dynamic behavior of the system from experiment and theory under periodic forcing, studied the strongly modulated response (SMR) of the system, and determined the range of NES parameters and excitation amplitude when high amplitude detached resonant tongue does not occur. The experimental results are

Z. Zhang · Z.-T. Gao · B. Fang · Y.-W. Zhang (✉)  
College of Aerospace Engineerings, Shenyang Aerospace  
University, Shenyang 110136, China  
e-mail: zhangyewei1218@126.com

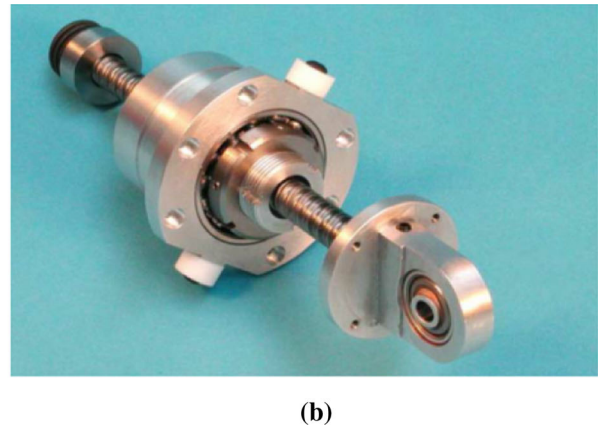
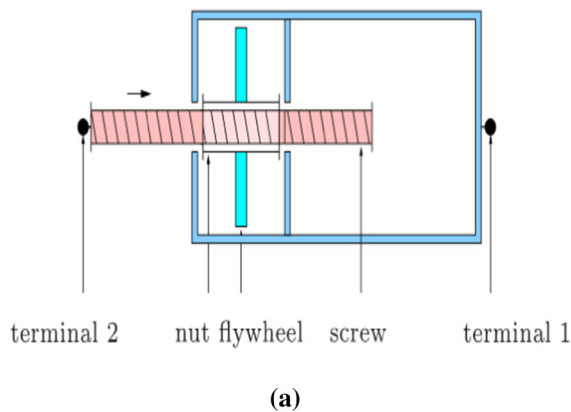


**Fig. 1** Ball screw inerter: **a** Model schematic diagram; **b** photo of an inerter [25]

basically consistent with the theoretical prediction [6]. Without doubt, NES is promising, and it has seen much practical application, being applied in many engineering fields [7]. In space-flight applications, for example, NES plays an important role in vibration suppression [8, 9]. For applications in civil engineering, Wang developed a two-phase NES for vibration suppression of foundation structures, and its vibration control efficiency is high [10]. In other research, a combination of theory and experiment has shown the effectiveness of NES in vibration suppression [11]. Both theoretically and experimentally, Chen showed that the results are more accurate when NES weight is considered in the vibration process [12]. A linear system coupled with NES can achieve good vibration suppression, and its parameters have been considered [13]. Zhang found that NES, along with NiTiNOL-steel wire ropes, can effectively suppress vibration of a whole satellite system [14]. Lu reviewed and compared three types of nonlinear dissipative devices, NES, PID, and NVD [15]. Bitar proved the existence of a third vibration harmonic, and improved the approximation by an extended complexity method [16]. As research on nonlinear energy sinks intensifies, some new nonlinear energy sinks stand out, such as NES with nontraditional nonlinear restoring forces [17], a rotating NES [18], a pendulum type NES [19], a hysteretic NES [20], a tuned bistable NES [21], a hybrid vibro-impact NES [22], and a lever type NES [23]. However, mass remains the central inertial element for most NESs, and large mass is a problem of that often hinders the engineering applications. It is therefore of significance and value to conduct research

on small-mass NESs for use in scientific research and in some engineering application.

An inerter is a particular kind of mechanical element that provides inertial parameters. It was first proposed by Smith of Cambridge University and named inerter [24]. It has two connecting terminals, which can be used as inertial components with mass. But unlike a simple massive object, an inerter can provide a much larger inertial mass than is suggested by its mass alone, and its inertia can be adjusted.

As an example, a ball screw inerter is shown in Fig. 1.

The principal formula of a nut rotating ball screw inerter is

$$b = \left(\frac{2\pi}{p}\right)^2 \cdot J \quad (1)$$

where  $p$  is the pitch of the inerter's lead screw,  $J$  is the moment of inertia of its flywheel, and  $b$  is the inertial mass, expressed in kg. The physical properties of an inerter are similar to those of a mass block with a mass equal to the inerter's inertia. According to Eq. (1), the inertial mass produced in the process of flywheel rotation is amplified by the inerter, so that an inertial mass of hundreds of kilograms can be achieved with a small flywheel of much less mass. For example, the mass of a ball screw inerter might be only 1 kg, yet its inertial mass can be adjusted to be 100 kg, providing favorable conditions for practical application.

Because of this characteristic, inerters have been widely studied, for instance in research on grounding of stay cables [26]. Zhang proposed a new inertial enhanced NES and showed that an optimal inertia falls

within a certain range [27]. However, there remains a significant mass problem in traditional NESs. Zhang proposed an inerter nonlinear energy sink, which overcomes the defects of large mass in traditional NES, and showed that the inerter nonlinear energy sinks have higher damping performance and much smaller mass than traditional NES [28].

For vibration control of elastic structures, Yang used NES to suppress excessive vibration of a pipeline and showed that the effectiveness of NES in this application [29]. Mamaghani studied the effect of a smooth NES on vibration suppression of a fixed pipe [30]. An impact damper has also been used in analysis of vibration suppression in a cantilever beam, and the results show that it can effectively suppress multiple resonance peaks [31]. The Galerkin truncation analysis of a Timoshenko beam is reported in ref. [32]. For the condition of 3:1 internal resonance, Ding studied the steady-state periodic response of the forced vibration of a moving viscoelastic beam [33]. A nonlinear vibration isolation system with three linear springs has also been found to effectively suppress lateral vibrations [34]. Considering non-ideal boundary support of the beam, the effect of nonlinear stiffness on the vibration suppression of NES has been discussed [35]. Zang also proposed a generalized transitivity method for NES evaluation [36].

Taking advantage of vibration suppression, an energy acquisition system can concentrate energy. Lu's studies of a bistable energy collection mechanism indicate that a horizontal spring is better than combined horizontal and vertical springs [37]. In dynamics and acoustics, strong nonlinearity can also lead to cross scale energy scattering [38]. Li studied the coupling of nonlinear energy sinks and energy collectors [39]. Researchers have shown great interest in the energy acquisition of piezoelectric structure with NES. NES vibration reduction analysis applied to beam structure has been studied more and more deeply. For linear beams with different boundary conditions, the robustness of the optimized NES has been analyzed by Parseh [40]. Under the action of an impact damper, a cantilever beam and the impact mass can collide repeatedly to reduce vibration [41]. Taking temperature and humidity into account, NES can also effectively suppress the nonlinear vibration of composite beam [42]. It can be seen from a wide range of research that NES applied to elastic structures can effectively suppress vibration. Neglecting geometric

nonlinearity, some researchers have revealed the vibration characteristics of beams with elastic supports. Zhang installed ten springs at each end of a pipeline [43]. Li uses a semi-analytical method to analyze the natural frequencies and mode shapes of an undamped double-beam system with arbitrary boundary conditions [44]. Ding was the first to discuss axially moving beams with generalized boundary conditions [45]. The dynamic stiffness matrices of axially moving Timoshenko beams and Euler Bernoulli beams with generalized boundary conditions have been established. Wang analyzed the vibration of a nonlinear support beam under harmonic force, and used a cubic spring to simulate the nonlinear elastic boundary [46]. Zang coupled two lever type NESs at the boundary of elastic beam, which proved the effectiveness of lever type NES [47]. Zhang coupled an inertial nonlinear energy sink at the boundary of an elastic beam, and showed that an inertial nonlinear energy sink has good damping effect [48]. However, in engineering applications, large displacement often exists in structural vibration, and the geometric nonlinearity of elastic beams cannot be ignored. Ding proved the necessity of bending vibration and elastic support for structural vibration isolation, and considered the geometric nonlinear characteristics of the beam [49]. Considering geometric nonlinearity, the resonance of asymmetric elastic boundary beam has been analyzed [50]. Based on a stable steady-state response with an initial condition of 0.0001, Ding defined and gave the flexural vibration transmissibility of an elastic beam while considering the geometric nonlinearity of beam transverse vibrations [51].

Mao first studied the nonlinear response of flexible structures under general nonlinear support conditions, and analyzed the boundary nonlinearity in detail. It was found that boundary nonlinearity played an important role in structural response [52]. A simple technique of passive vibration isolation for traditional flexible structures by nonlinear boundary has also been studied [53].

In the work reported here, a nonlinear boundary with inertial nonlinear energy sink (I-NES) is placed at the elastic boundaries of a beam, and the geometric nonlinearity of the beam in transverse vibration is studied. The influence of geometric nonlinearity of the beam on the system response and vibration-suppression effect under foundation excitation is the principal focus, and it is compared with the system vibration

response in the absence of geometric nonlinearity. The results show that I-NESs with elastic boundaries can effectively suppress transverse vibration of the beam when the geometric nonlinearity of the beam is considered, and optimized I-NESs can reduce the vibration of the beam by 96%.

### 2 Dynamic model under foundation excitation

The dynamic model of an elastic beam with vertical spring supports at both ends is shown in Fig. 2, and takes into account its geometric nonlinearity. The quantities  $L$ ,  $T$  and  $X$  are length, time and axial coordinate, respectively.  $K_L$  and  $K_R$  are the stiffnesses of the left and right vertical springs. Only the transverse displacement of the beam is considered, which is described as  $W(X, T)$ . The beam is excited by displacement from its foundation at both ends. This displacement excitation is described as  $U(T) = U_0 \cos(\Omega \cdot T)$ , where  $U_0$  and  $\Omega$  are, respectively, the amplitude and frequency of the displacement excitation. I-NESs are coupled to the elastic boundaries at both ends of the beam. The inertial masses of the I-NESs of the left and right ends are expressed by  $b_{NL}$  and  $b_{NR}$ . The linear dampings of the I-NESs at the left and right ends are expressed by  $c_{NL}$  and  $c_{NR}$ . And the cubic nonlinearities of the I-NESs of the left and right ends are expressed by  $k_{NL}$  and  $k_{NR}$ . The inerter can provide larger inertia with small mass, which makes up for the defects of a massive NES. The displacements of the I-NESs at the left and right ends are expressed by  $U_{NL}(T)$  and  $U_{NR}(T)$ .

Based on the generalized Hamilton’s principle, variational method and partial integration method, the dynamic equation of the system is

$$\int_0^L \left[ \rho A W_{,TT} + EI W_{,XXXX} + \Lambda I W_{,XXXXT} - \frac{3}{2} E A W_{,X}^2 W_{,XX} \right] dX + \left[ -K_L U_0 \cos(\Omega T) + \eta_L \Omega U_0 \sin(\Omega T) + k_{NL} (W_L - U_{NL})^3 + c_{NL} (W_{L,X} - U_{NL,T}) \right] \delta(X) + \left[ -K_R U_0 \cos(\Omega T) + \eta_R \Omega U_0 \sin(\Omega T) + k_{NR} (W_R - U_{NR})^3 + c_{NR} (W_{R,X} - U_{NR,T}) \right] \delta(X - L) = 0 \tag{2}$$

where  $W_L$  and  $W_R$  are the displacement of the left and right boundaries of the beam.

The dynamic equations for the I-NESs are expressed as

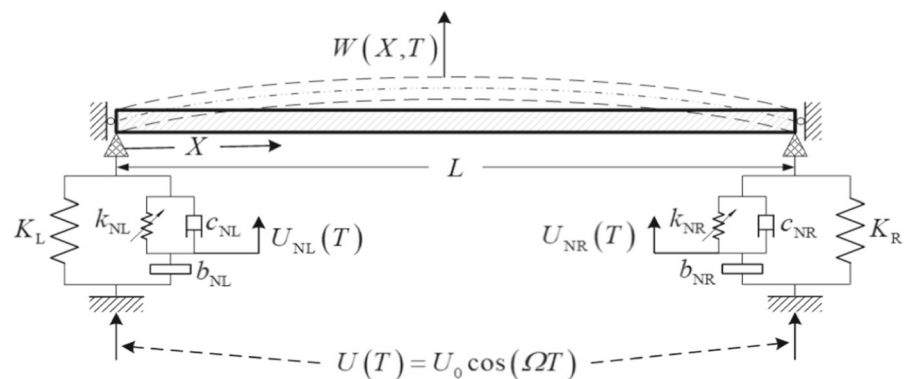
$$\begin{aligned} b_{NL} [U_{NL,TT} + \Omega^2 U_0 \cos(\Omega T)] + k_{NL} (U_{NL} - W_L)^3 + c_{NL} (U_{NL,T} - W_{L,T}) &= 0, \\ b_{NR} [U_{NR,TT} + \Omega^2 U_0 \cos(\Omega T)] + k_{NR} (U_{NR} - W_R)^3 + c_{NR} (U_{NR,T} - W_{R,T}) &= 0 \end{aligned} \tag{3}$$

The boundary conditions of the elastic beam are

$$\begin{aligned} W_{L,XX} &= 0, \quad EI W_{L,XXX} = -K_L W_L, \\ W_{R,XX} &= 0, \quad EI W_{R,XXX} = K_R W_R \end{aligned} \tag{4}$$

In dimensionless form, the dynamic equation of the system is

Fig. 2 Model of the beam



$$\begin{aligned}
 & \int_0^1 [w_{,tt}(x, t) + \kappa^2 w_{,xxxx}(x, t) + \kappa^2 \lambda w_{,xxxxt}(x, t) \\
 & - \frac{3}{2} w_{,x}^2(x, t) w_{,xx}(x, t)] dx + [\kappa_{NL}(w_L - u_{NL})^3 \\
 & + \zeta_{NL}(w_{L,t} - u_{NL,t}) - u_L \cos(\omega t)] \delta(0) \\
 & + [\kappa_{NR}(w_R - u_{NR})^3 + \zeta_{NR}(w_{R,t} - u_{NR,t}) \\
 & - u_R \cos(\omega t)] \delta(1) = 0
 \end{aligned} \tag{5}$$

The dimensionless boundary conditions are

$$\begin{aligned}
 w_{,xx}(0, t) = 0, \quad w_{,xxx}(0, t) = -\kappa_L w_L, \\
 w_{,xx}(1, t) = 0, \quad w_{,xxx}(1, t) = \kappa_R w_R
 \end{aligned} \tag{6}$$

Also in dimensionless form, the dynamic equations of the I-NESs are

$$\begin{aligned}
 \mu_{NL} \cdot u_{NL,tt} + \kappa_{NL}(u_{NL} - w_L)^3 + \zeta_{NL}(u_{NL,t} - w_{L,t}) \\
 + \mu_{NL} u_0 \omega^2 \cos(\omega t) = 0, \\
 \mu_{NR} \cdot u_{NR,tt} + \kappa_{NR}(u_{NR} - w_R)^3 + \zeta_{NR}(u_{NR,t} - w_{R,t}) \\
 + \mu_{NR} u_0 \omega^2 \cos(\omega t) = 0
 \end{aligned} \tag{7}$$

where

$$\begin{aligned}
 x = \frac{X}{L}, w = \frac{W}{L}, w_L = \frac{W_L}{L}, w_R = \frac{W_R}{L}, u_{NL} = \frac{U_{NL}}{L}, \\
 u_{NR} = \frac{U_{NR}}{L}, t = \frac{T}{L} \sqrt{\frac{E}{\rho}}, \omega = \Omega L \sqrt{\frac{\rho}{E}}, \\
 \kappa = \frac{1}{L} \sqrt{\frac{I}{A}}, \lambda = \frac{\Lambda}{L} \sqrt{\frac{1}{E\rho}}, \kappa_L = \frac{K_L L^3}{EI}, \kappa_R = \frac{K_R L^3}{EI}, \\
 u_L = \frac{K_L}{EA} U_0, \\
 u_R = \frac{K_R}{EA} U_0, u_0 = \frac{U_0}{L}, \mu_{NL} = \frac{b_{NL}}{\rho AL}, \mu_{NR} = \frac{b_{NR}}{\rho AL}, \\
 \kappa_{NL} = \frac{L^3}{EA} k_{NL}, \zeta_{NL} = \frac{c_{NL}}{A} \sqrt{\frac{1}{E\rho}}, \kappa_{NR} = \frac{L^3}{EA} k_{NR}, \\
 \zeta_{NR} = \frac{c_{NR}}{A} \sqrt{\frac{1}{E\rho}}
 \end{aligned} \tag{8}$$

The material of the elastic beam is aluminum alloy; the physical and geometric parameters of the system are shown in Table 1. It is worth noting that the inertial mass is  $b_N = 0.084$  kg, while the actual mass is  $m_b = 0.00084$  kg. The dimensionless parameters calculated based on Eq. 8 are shown in Table 2.

### 3 Steady-state response under foundation excitation

According to the parameters in Table 1, the modal function of the beam with elastic support boundaries is

**Table 1** system dimensional parameter

Parameter name	Symbol	Value
Young's modulus	$E$	68.9 GPa
Density	$\rho$	2800 kg/m <sup>3</sup>
Viscoelasticity	$A$	$4 \times 10^6$ N s/m <sup>2</sup>
Length	$L$	1 m
Width	$b$	0.02 m
Hight	$h$	0.01 m
Cross-sectional area	$A$	$2 \times 10^{-4}$ m <sup>2</sup>
Cross-sectional moment of inertia	$I$	$1.67 \times 10^{-9}$ m <sup>4</sup>
Inertial mass	$b_{NL} = b_{NR}$	0.084 kg
Mass of the inerter	$m_{NL} = m_{NR}$	0.00084 kg
Cubic nonlinearity	$k_{NL} = k_{NR}$	$5 \times 10^7$ N/m <sup>3</sup>
Damping	$c_{NL} = c_{NR}$	1 N·s/m
Linear vertical stiffness on the left	$K_L$	5753.15 N/m
Linear vertical stiffness on the right	$K_R$	5753.15 N/m

**Table 2** System dimensionless parameter

Parameter name	Symbol	Value
Flexural coefficient	$\kappa$	0.0028896
Viscoelasticity coefficient	$\lambda$	0.288
Vertical spring coefficient	$kL = kR$	50
Inertance ratio	$\mu_{NL} = \mu_{NR}$	0.15
Nonlinearity coefficient	$\kappa_{NL} = \kappa_{NR}$	3.63
Damping coefficient	$\zeta_{NL} = \zeta_{NR}$	0.00036

shown in Eq. (9). Therefore, the first four modal modes of the beam with elastic support boundaries are illustrated in Fig. 3. In Fig. 3, it can be found that the maximum displacement of the first mode appears at the midpoint of the beam, and the maximum displacement of the third mode appears at the boundaries of the beam. In addition, it can be found that the first and third modes of the elastic beam are symmetrically distributed with respect to the midpoint of the beam, while the second and fourth modes are antisymmetrically distributed with respect to the midpoint. Therefore, in the remainder of this paper, only the left boundary and the midpoint of the beam are considered.

$$\begin{aligned}
 \phi_1(x) &= \cos(2.6844x) + 4.2977 \cdot \sin(2.6844x) \\
 &\quad + ch(2.6844x) - 0.8722 \cdot sh(2.6844x), \\
 \phi_2(x) &= \cos(4.0392x) + 0.4816 \cdot \sin(4.0392x) \\
 &\quad + ch(4.0392x) - 1.0359 \cdot sh(4.0392x), \\
 \phi_3(x) &= \cos(5.5242x) - 0.3989 \cdot \sin(5.5242x) \\
 &\quad + ch(5.5242x) - 0.9921 \cdot sh(5.5242x), \\
 \phi_4(x) &= \cos(8.0633x) - 0.8099 \cdot \sin(8.0633x) \\
 &\quad + ch(8.0633x) - 1.0006 \cdot sh(8.0633x)
 \end{aligned} \tag{9}$$

### 3.1 The Galerkin method

The partial differential equations (5) and (7) can be truncated by using the Galerkin method. The Runge–Kutta numerical method takes the fourth order into account. Then, it is used to solve the time response of the system.

It is assumed that the approximate solution of the transverse vibration displacement of the beam is

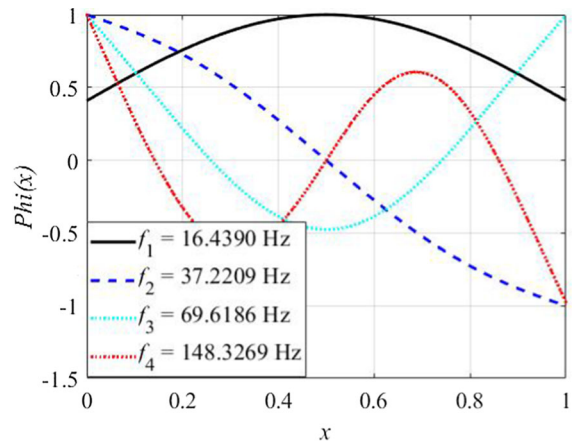


**Fig. 3** The first four modal modes of the beam with elastic support boundaries

$$w(x, t) = \sum_{n=1}^N \phi_n(x)q_n(t) \tag{10}$$

where  $n$  is a positive integer,  $\phi_n(x)$  is the modal function of the beam, and  $q_n(t)$  is the generalized displacement of the transverse vibration. The potential function and the weight function of the Galerkin method are chosen as the modal functions of the beam. The ordinary differential equation can be expressed as

$$\begin{aligned}
 &\int_0^1 \sum_{n=1}^N \phi_n(x)\ddot{q}_n(t)\psi_m(x)dx + \kappa^2 \int_0^1 \sum_{n=1}^N \phi_n^{(4)}(x)q_n(t)\psi_m(x)dx \\
 &- \frac{3}{2} \int_0^1 \left( \sum_{n=1}^N \phi_n(x)\dot{q}_n(t) \right)^2 \sum_{n=1}^N \phi_n(x)q_n(t)\psi_m(x)dx \\
 &+ \kappa^2 \lambda \int_0^1 \sum_{n=1}^N \phi_n^{(4)}(x)\dot{q}_n(t)\psi_m(x)dx \\
 &+ \left\{ \kappa_{NL} \left[ \sum_{n=1}^N \phi_n(0)q_n(t) - u_{NL}(t) \right]^3 \right. \\
 &+ \zeta_{NL} \left[ \sum_{n=1}^N \phi_n(0)\dot{q}_n(t) - \dot{u}_{NL}(t) \right] \left. \right\} \psi_m(0) \\
 &+ \left\{ \kappa_{NR} \left[ \sum_{n=1}^N \phi_n(1)q_n(t) - u_{NR}(t) \right]^3 \right. \\
 &+ \zeta_{NR} \left[ \sum_{n=1}^N \phi_n(1)\dot{q}_n(t) - \dot{u}_{NR}(t) \right] \left. \right\} \psi_m(1) \\
 &- u_L \cos(\omega t)\psi_m(0) - u_R \cos(\omega t)\psi_m(1) = 0
 \end{aligned} \tag{11}$$

$$\begin{aligned}
 &\mu_{NL}\ddot{u}_{NL}(t) + \kappa_{NL} \left[ u_{NL}(t) - \sum_{n=1}^N \phi_n(0)q_n(t) \right]^3 \\
 &\quad + \zeta_{NL} \left[ \dot{u}_{NL}(t) - \sum_{n=1}^N \phi_n(0)\dot{q}_n(t) \right] \\
 &\quad + \mu_{NL}u_0\omega^2 \cos(\omega t) = 0, \\
 &\mu_{NR}\ddot{u}_{NR}(t) + \kappa_{NR} \left[ u_{NR}(t) - \sum_{n=1}^N \phi_n(1)q_n(t) \right]^3 \\
 &\quad + \zeta_{NR} \left[ \dot{u}_{NR}(t) - \sum_{n=1}^N \phi_n(1)\dot{q}_n(t) \right] \\
 &\quad + \mu_{NR}u_0\omega^2 \cos(\omega t) = 0
 \end{aligned} \tag{12}$$

where  $m = 1, 2, 3, 4$ , and

$$\begin{aligned}
 \int_0^1 \phi_n(x)\psi_m(x)dx &= 0, \quad n \neq m, \\
 \int_0^1 \phi_n^{(4)}(x)\psi_m(x)dx &= 0, \quad n \neq m
 \end{aligned} \tag{13}$$

Therefore, Eq. (11) can be written as

$$\begin{aligned}
 &M_m\ddot{q}_m(t) + \kappa^2 K_m q_m(t) + \lambda \kappa^2 K_m \dot{q}_m(t) - \frac{3}{2} D_m q_m(t)^3 \\
 &\quad + \left\{ \kappa_{NL} \left[ \sum_{n=1}^N \phi_n(0)q_n(t) - u_{NL}(t) \right]^3 + \zeta_{NL} \left[ \sum_{n=1}^N \phi_n(0)\dot{q}_n(t) - \dot{u}_{NL}(t) \right] \right\} \psi_m(0) \\
 &\quad + \left\{ \kappa_{NR} \left[ \sum_{n=1}^N \phi_n(1)q_n(t) - u_{NR}(t) \right]^3 + \zeta_{NR} \left[ \sum_{n=1}^N \phi_n(1)\dot{q}_n(t) - \dot{u}_{NR}(t) \right] \right\} \psi_m(1) \\
 &\quad - u_L \cos(\omega t)\psi_m(0) - u_R \cos(\omega t)\psi_m(1) = 0
 \end{aligned} \tag{14}$$

where

$$\begin{aligned}
 M_m &= \int_0^1 \phi_m(x)\psi_m(x)dx, \quad K_m = \int_0^1 \phi_m^{(4)}(x)\psi_m(x)dx, \\
 D_m &= \int_0^1 \dot{\phi}_m^2(x)\ddot{\phi}_m(x)\psi_m(x)dx
 \end{aligned} \tag{15}$$

The initial values are set as follows:

$$\begin{aligned}
 q_1 &= 0, \quad \dot{q}_1 = 0, \quad q_j = 0, \quad \dot{q}_j = 0, \quad j = 2, 3, 4 \\
 u_{NL} &= u_{NR} = 0, \quad \dot{u}_{NL} = \dot{u}_{NR} = 0
 \end{aligned} \tag{16}$$

For the second-, fourth-, and sixth-order Galerkin truncation, from the time histories under different excitation frequencies, the amplitude frequency response curves of the numerical solutions of the system can be extracted. The steady-state amplitude-frequency response curves of the numerical solution are illustrated in Fig. 4.  $A(0)$  represents the amplitude of the left boundary of the beam, and  $A(L/2)$  represents the amplitude of the midpoint of the beam. In Fig. 4,

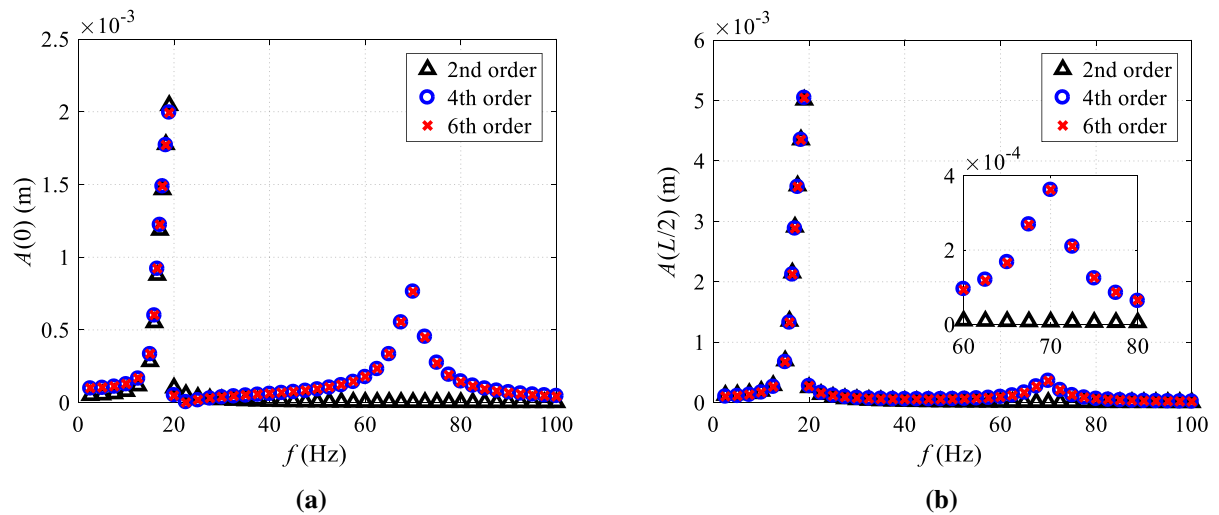


**Fig. 4** Amplitude frequency response curves of the system for different Galerkin truncation orders: **a** The left boundary:  $X = 0$ ; **b** The midpoint:  $X = L/2$

the results of fourth- and sixth-order Galerkin truncation almost coincide. At the third-order main resonance, the second-order Galerkin truncation does not show a resonance peak. Therefore, the fourth-order Galerkin truncation is used in the following studies. In Fig. 4, it can also be observed that there is an obvious nonlinear hardening phenomenon and the jump phenomenon at the first-order main resonance of the system.

### 3.2 The harmonic balance method

The ordinary differential equations obtained by Galerkin truncation can be solved by the harmonic balance method. Considering that the governing equations contain cubic nonlinearity, only odd terms are considered when assuming harmonic solutions. The order of Galerkin truncation is expressed by  $m$ , and the harmonic order is expressed by  $h$ . Suppose, then, that the harmonic solutions are

$$\begin{aligned}
 q_m &= \sum_{i=0}^h \{ a_{m,2i+1} \cos[(2i + 1)\omega t] + b_{m,2i+1} \sin[(2i + 1)\omega t] \}, \\
 u_{NL} &= \sum_{i=0}^h \{ a_{L,2i+1} \cos[(2i + 1)\omega t] + b_{L,2i+1} \sin[(2i + 1)\omega t] \}, \\
 u_{NR} &= \sum_{i=0}^h \{ a_{R,2i+1} \cos[(2i + 1)\omega t] + b_{R,2i+1} \sin[(2i + 1)\omega t] \}
 \end{aligned} \tag{17}$$

Taking the first harmonic assumption as an example, the dynamic equation of the beam coupled with I-NESs is

$$\begin{aligned}
 M_1 \ddot{q}_1 + K_1 q_1 + C_1 \dot{q}_1 - \frac{3}{2} D_1 \dot{q}_1^3 \\
 + \left[ \kappa_{NL} (\phi_{L,1} q_1 - u_{NL})^3 + \zeta_{NL} (\phi_{L,1} \dot{q}_1 - \dot{u}_{NL}) \right] \psi_{L,1} \\
 + \left[ \kappa_{NR} (\phi_{R,1} q_1 - u_{NR})^3 + \zeta_{NR} (\phi_{R,1} \dot{q}_1 - \dot{u}_{NR}) \right] \psi_{R,1} \\
 - u_L \cos(\omega t) \psi_{L,1} - u_R \cos(\omega t) \psi_{R,1} = 0
 \end{aligned} \tag{18}$$

$$\begin{aligned}
 \mu_{NL} \ddot{u}_{NL} + \kappa_{NL} (u_{NL} - \phi_{L,1} q_1)^3 + \zeta_{NL} (\dot{u}_{NL} - \phi_{L,1} \dot{q}_1) \\
 + \mu_{NL} u_0 \omega^2 \cos(\omega t) = 0, \\
 \mu_{NR} \ddot{u}_{NR} + \kappa_{NR} (u_{NR} - \phi_{R,1} q_1)^3 + \zeta_{NR} (\dot{u}_{NR} - \phi_{R,1} \dot{q}_1) \\
 + \mu_{NR} u_0 \omega^2 \cos(\omega t) = 0
 \end{aligned} \tag{19}$$

where  $\phi_{L,1} = \phi_1(0)$ ,  $\psi_{L,1} = \psi_1(0)$ ,  $\phi_{R,1} = \phi_1(1)$ ,  $\psi_{R,1} = \psi_1(1)$ .

Suppose the solution of the first harmonic is

$$\begin{aligned}
 q_1 &= a_{1,1} \cos(\omega t) + b_{1,1} \sin(\omega t), \\
 \mu_{NL} &= a_{L,1} \cos(\omega t) + b_{L,1} \sin(\omega t), \\
 \mu_{NR} &= a_{R,1} \cos(\omega t) + b_{R,1} \sin(\omega t)
 \end{aligned} \tag{20}$$

By substituting Eq. (20) into equation Eq. (18) and sorting out the coefficient equations corresponding to each order of harmonics, the following algebraic equations are obtained.

$$\begin{aligned}
 (12a_{1,1}^3 - 1.5a_{L,1}^3 - 18a_{1,1}^2 a_{L,1} + 9a_{1,1} a_{L,1}^2 + 12a_{1,1} b_{L,1}^2 \\
 + 3a_{1,1} b_{L,1}^2 - 6a_{L,1} b_{1,1}^2 \\
 - 12a_{1,1} b_{1,1} b_{L,1} + 6a_{L,1} b_{1,1} b_{L,1} - 1.5a_{L,1} b_{L,1}^2) \kappa_{NL} \\
 + (12a_{1,1}^3 - 1.5a_{R,1}^3 - 18a_{1,1}^2 a_{R,1} \\
 + 9a_{1,1} a_{R,1}^2 + 12a_{1,1} b_{R,1}^2 + 3a_{1,1} b_{R,1}^2 - 6a_{R,1} b_{1,1}^2 \\
 - 12a_{1,1} b_{1,1} b_{R,1} + 6a_{R,1} b_{1,1} b_{L,1} \\
 - 1.5a_{R,1} b_{L,1}^2) \kappa_{NR} + 32174.37508a_{1,1}^3 \\
 - 15.63232450a_{1,1} \omega^2 + 811.6820390 \\
 a_{1,1} \kappa^2 + 4\zeta_{NR} b_{1,1} \omega + 4\zeta_{NL} b_{1,1} \omega \\
 + 811.6820390 \kappa^2 b_{1,1} \omega + 32174.37508a_{1,1} \\
 b_{1,1}^2 - 2u_L - 2u_R - 2\zeta_{NL} b_{L,1} \omega - 2\zeta_{NR} b_{R,1} \omega = 0, \\
 (12a_{1,1}^2 b_{1,1} - 6a_{1,1}^2 b_{L,1} + 3a_{1,1}^2 b_{R,1} - 1.5a_{L,1}^2 b_{L,1} \\
 - 18b_{1,1}^2 b_{L,1} + 9b_{1,1} b_{L,1}^2 + 12b_{1,1}^3 \\
 - 12a_{1,1} a_{L,1} b_{1,1} + 6a_{1,1} a_{L,1} b_{L,1} - 1.5b_{L,1}^3) \kappa_{NL} \\
 + (12a_{1,1}^2 b_{1,1} - 6a_{1,1}^2 b_{R,1} + 3a_{1,1}^2 b_{L,1} \\
 - 1.5a_{R,1}^2 b_{R,1} - 18b_{1,1}^2 b_{R,1} + 9b_{1,1} b_{R,1}^2 \\
 + 12b_{1,1}^3 - 12a_{1,1} a_{R,1} b_{1,1} + 6a_{1,1} a_{R,1} b_{L,1} \\
 - 1.5b_{R,1}^3) \kappa_{NR} + 32174.37508b_{1,1}^3 \\
 - 15.63232450b_{1,1} \omega^2 + 811.6820390 \\
 b_{1,1} \kappa^2 + 2\zeta_{NL} a_{L,1} \omega + 2\zeta_{NR} a_{R,1} \omega \\
 - 811.6820390 \kappa^2 a_{1,1} \omega + 32174.37508a_{1,1}^2 \\
 b_{1,1} - 4\zeta_{NR} a_{1,1} \omega - 4\zeta_{NL} a_{1,1} \omega, \\
 (6a_{1,1} b_{1,1} b_{L,1} - 3a_{L,1} b_{1,1} b_{L,1} + 9a_{1,1}^2 a_{L,1} \\
 - 4.5a_{1,1} a_{L,1}^2 - 6a_{1,1}^2 + 0.75a_{L,1}^2 - 6a_{1,1} b_{L,1}^2 \\
 - 1.5a_{1,1} b_{L,1}^2 + 3a_{L,1} b_{1,1}^2 + 0.75a_{L,1} b_{L,1}^2) \kappa_{NL} \\
 - \omega^2 a_{L,1} \mu_{NL} + \mu_{NL} u_0 \omega^2 - 2\zeta_{NL} b_{1,1} \omega \\
 + \zeta_{NL} b_{L,1} \omega = 0, \\
 (-6b_{1,1}^3 + 0.75b_{L,1}^3 - 6a_{1,1}^2 b_{1,1} + 3a_{1,1}^2 b_{L,1} \\
 - 1.5a_{1,1}^2 b_{1,1} + 0.75a_{L,1}^2 b_{L,1} + 6a_{1,1} a_{L,1} b_{1,1} \\
 - 3a_{1,1} a_{L,1} b_{L,1} + 9b_{1,1}^2 b_{L,1} - 4.5b_{1,1} b_{L,1}^2) \kappa_{NL} - \omega^2 b_{L,1} \mu_{NL} \\
 + 2\zeta_{NL} a_{1,1} \omega - \zeta_{NL} a_{L,1} \omega = 0, \\
 (6a_{1,1} b_{1,1} b_{R,1} - 3a_{R,1} b_{1,1} b_{R,1} + 9a_{1,1}^2 a_{R,1} - 4.5a_{1,1} a_{R,1}^2 - 6a_{1,1}^3 + 0.75a_{R,1}^3 - 6a_{1,1} b_{R,1}^2 \\
 - 1.5a_{1,1} b_{R,1}^2 + 3a_{R,1} b_{1,1}^2 + 0.75a_{R,1} b_{R,1}^2) \kappa_{NR} - \omega^2 a_{R,1} \mu_{NR} + \mu_{NR} u_0 \omega^2 - 2\zeta_{NR} b_{1,1} \omega \\
 + \zeta_{NR} b_{R,1} \omega = 0, \\
 (-6b_{1,1}^3 + 0.75b_{R,1}^3 - 6a_{1,1}^2 b_{1,1} + 3a_{1,1}^2 b_{R,1} - 1.5a_{1,1}^2 b_{1,1} + 0.75a_{R,1}^2 b_{R,1} + 6a_{1,1} a_{R,1} b_{1,1} \\
 - 3a_{1,1} a_{R,1} b_{R,1} + 9b_{1,1}^2 b_{R,1} - 4.5b_{1,1} b_{R,1}^2) \kappa_{NR} - \omega^2 b_{R,1} \mu_{NR} + 2\zeta_{NR} a_{1,1} \omega - \zeta_{NR} a_{R,1} \omega = 0
 \end{aligned} \tag{21}$$

Then the pseudo-arc-length algorithm can be used to solve the algebraic equations (21), and the amplitude frequency response of the system can be obtained. Here, assuming that the harmonic solution is of order 4. Using the same method, considering the cubic



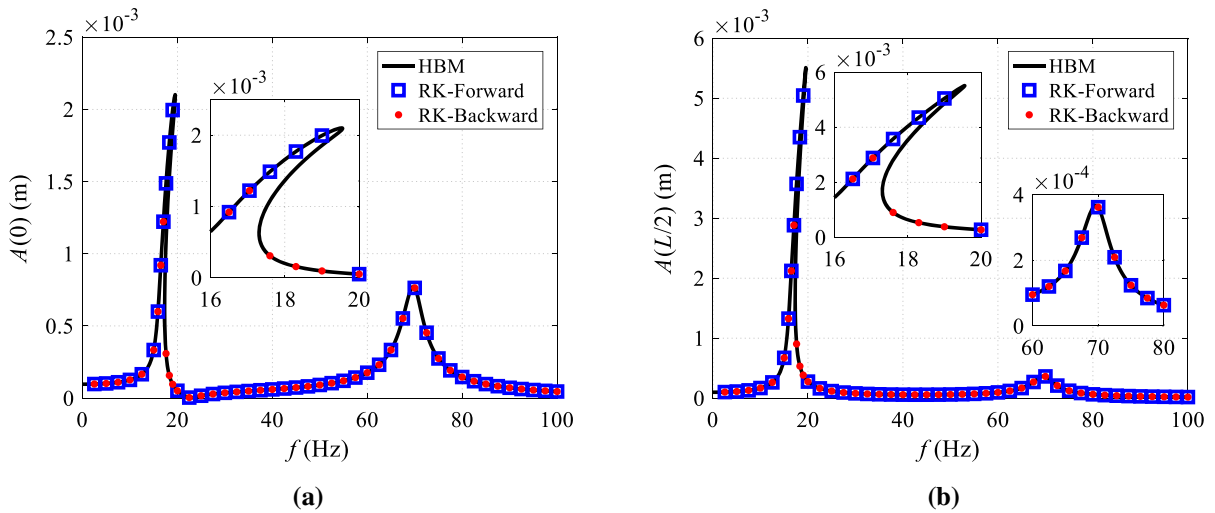


**Fig. 5** The analytical solution verified by numerical simulation: **a** The left boundary:  $X = 0$ ; **b** The midpoint:  $X = L/2$

nonlinearity in the equations and ignoring the influence of even order in the hypothetical solution, the steady-state amplitude frequency responses of the system can be obtained.

A comparison of the steady-state amplitude-frequency curves obtained by the harmonic balance method and the Runge–Kutta method is shown in Fig. 5. It can be seen from Fig. 5 that the numerical solution obtained by the Runge–Kutta method has only one steady-state solution. In the region of multiple steady-state solutions, all stable steady-state solutions can be obtained by the harmonic balance method. The forward and backward results of the Runge–Kutta method show an obvious nonlinear jump phenomenon at the first main resonance. Within a certain range, the approximate analytical results are basically consistent with the numerical solutions obtained by the Runge–Kutta method. This implies that the approximate analytical results are accurate and reliable.

#### 4 Vibration suppression analysis of I-NES with or without beam geometric nonlinearity

$A_u$  represents the amplitude of the main resonance of the uncoupled system, and  $A_c$  represents the amplitude of the main resonance of the coupled I-NES system. Therefore, the vibration suppression evaluation index of I-NES can be expressed as

$$R_A = \frac{A_u - A_c}{A_u} \times 100\% \tag{22}$$

#### 4.1 Free vibration response

Let  $q_1 = 0.5$  in Eq. (16) and the other initial values are still 0, the vibration suppression analysis for the free vibration response is shown in Fig. 6. As shown in Fig. 6, the time history curves of the uncontrolled linear beam and the uncontrolled geometrically nonlinear beam look to an exponential decay. However, the time history curves of the linear beam coupled I-NESs and the geometrically nonlinear beam coupled I-NESs show slopes linear decrease decay. This is the characteristic of nonlinear energy dissipation by NES. Moreover, it can be seen from this figure that the response amplitude caused by considering the geometric nonlinearity of the beam is significantly lower for both the uncoupled system and the coupled I-NES system than for the system without considering the geometric nonlinearity of the beam. This indicates that the geometric nonlinearity of the beam also affects the time-domain responses. Therefore, the geometric nonlinearity cannot be ignored. At the same time, on the premise of considering the geometric nonlinearity of the beam, I-NES can make the amplitude of the system attenuate rapidly, both at the left boundary and the midpoint of the beam, which has an obvious vibration suppression effect.

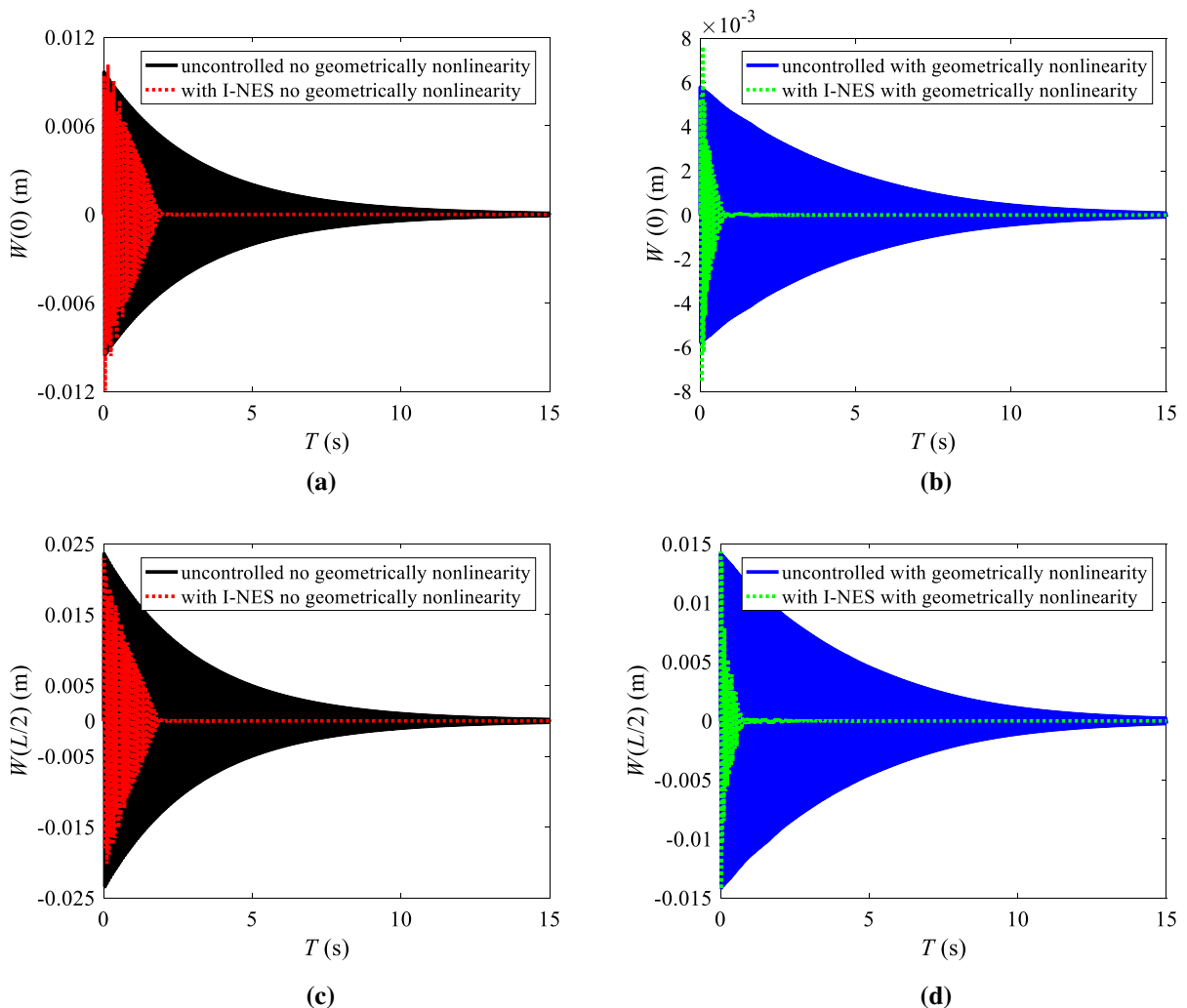


**Fig. 6** Transient response time history under initial displacement excitation: **a** The left boundary of a linear beam:  $X = 0$ ; **b** The left boundary of a geometrically nonlinear beam:  $X = 0$ ;

**c** The midpoint of a linear beam:  $X = L/2$ ; **d** The midpoint of a geometrically nonlinear beam:  $X = L/2$

#### 4.2 Steady-state response

In Figs. 7, 8, 9 and 10, the amplitudes of uncoupled I-NES system are compared whether the geometric nonlinear characteristics of beam are considered or not, and the amplitudes of coupled I-NES system are compared whether the geometric nonlinear characteristics of beam are considered or not. In order to better explain the influence of beam geometric nonlinearity on I-NES vibration suppression without considering the influence of external excitation amplitude, the excitation amplitude  $U_0$  is set to the same value. For  $U_0 = 0.0001$  m, the vibration suppression effects of

the I-NESs on the steady-state responses are shown in Table 3. Obviously, the I-NESs have a significant vibration suppression effect on the main resonance of the elastic beam. For the first-order main resonance of the left boundary, when the geometric nonlinearity of the beam is not considered, the vibration suppression percentage of the I-NESs is 76.53%. When the geometric nonlinearity of the beam is considered, the vibration suppression percentage of the I-NESs is 57.47%. For the first-order main resonance at the midpoint of the beam, when the geometric nonlinearity of the beam is not considered, the vibration suppression percentage of the I-NESs is

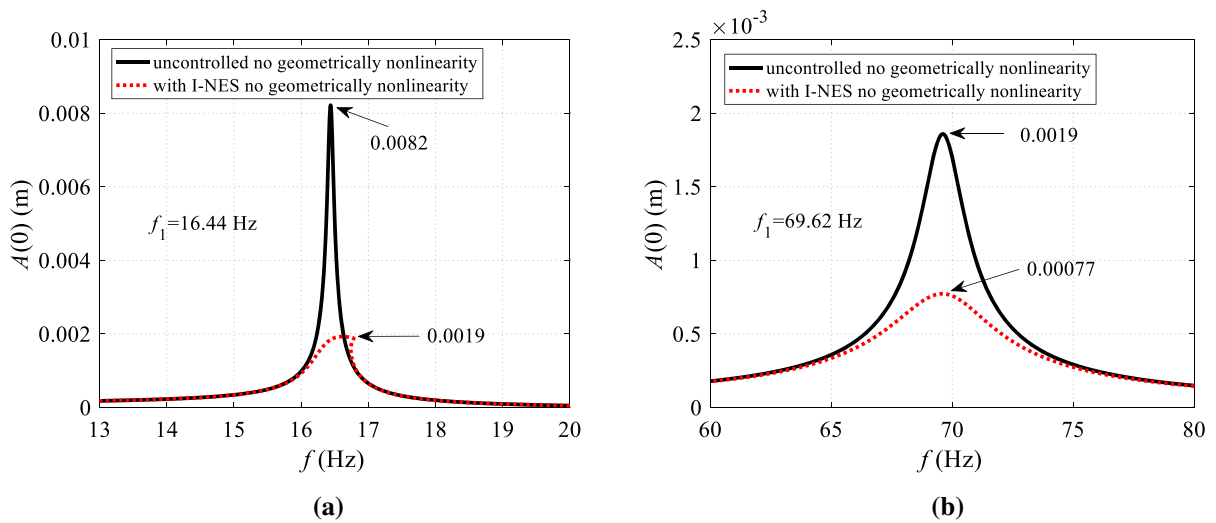


**Fig. 7** Vibration suppression analysis of I-NES at the left boundary of a linear beam: **a** The first-order main resonance:  $f_1 = 16.44$  Hz; **b** The third-order main resonance:  $f_3 = 69.62$  Hz

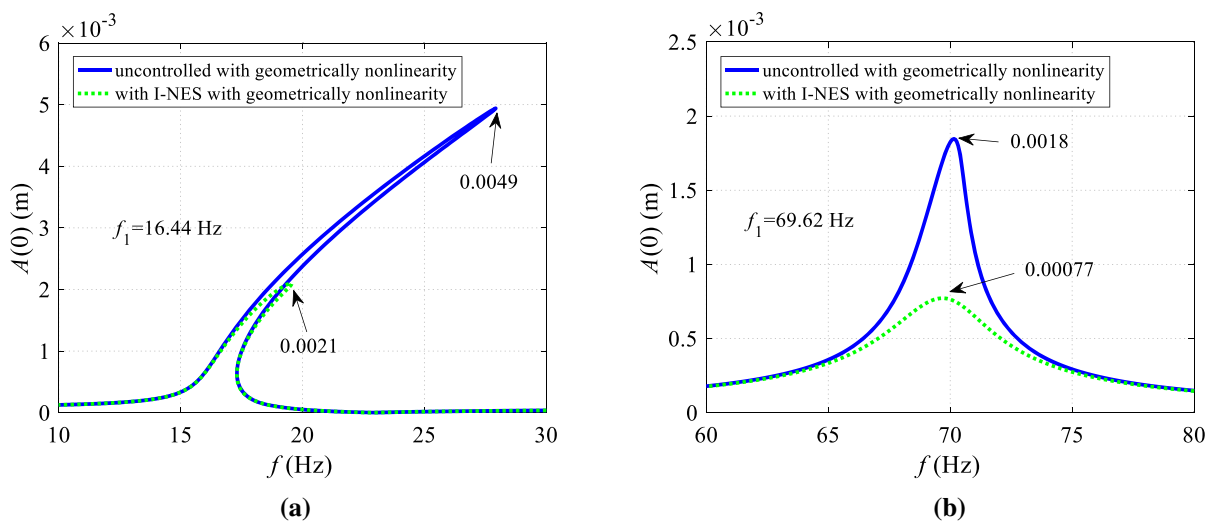


**Fig. 8** Vibration suppression analysis of I-NES at the left boundary of a geometrically nonlinear beam: **a** The first-order main resonance:  $f_1 = 16.44$  Hz; **b** The third-order main resonance:  $f_3 = 69.62$  Hz

74.99%. When the geometric nonlinearity of the beam is considered, the vibration suppression percentage of the I-NESs is 54.49%. It can be seen that the I-NESs have a very good vibration suppression effect whether the geometric nonlinearity is considered or not. As shown in Figs. 8a and 10a, when the geometric nonlinearity of the beam is considered, both the uncoupled and the coupled I-NESs system show strong nonlinear hardening characteristics. When Fig. 7a is compared with Figs. 8a, and 9a is compared

with Fig. 10a, it is seen that geometric nonlinearity leads to a significant reduction of the vibration amplitude of the beam. However, compared with the case without considering geometric nonlinearity, the vibration suppression of the I-NESs is reduced. Therefore, the geometric nonlinearity of the beam cannot be ignored in the process of engineering research.

For the third-order main resonance of the left boundary of a beam, when the geometric nonlinearity

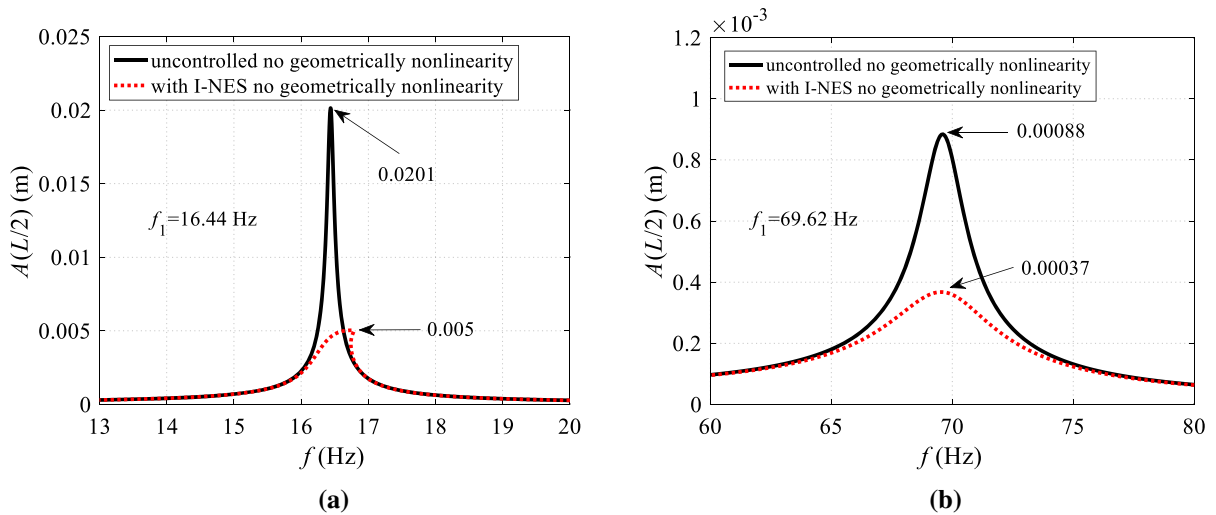


**Fig. 9** Vibration suppression analysis of I-NES at the midpoint of a linear beam: **a** The first-order main resonance:  $f_1 = 16.44$  Hz; **b** The third-order main resonance:  $f_3 = 69.62$  Hz

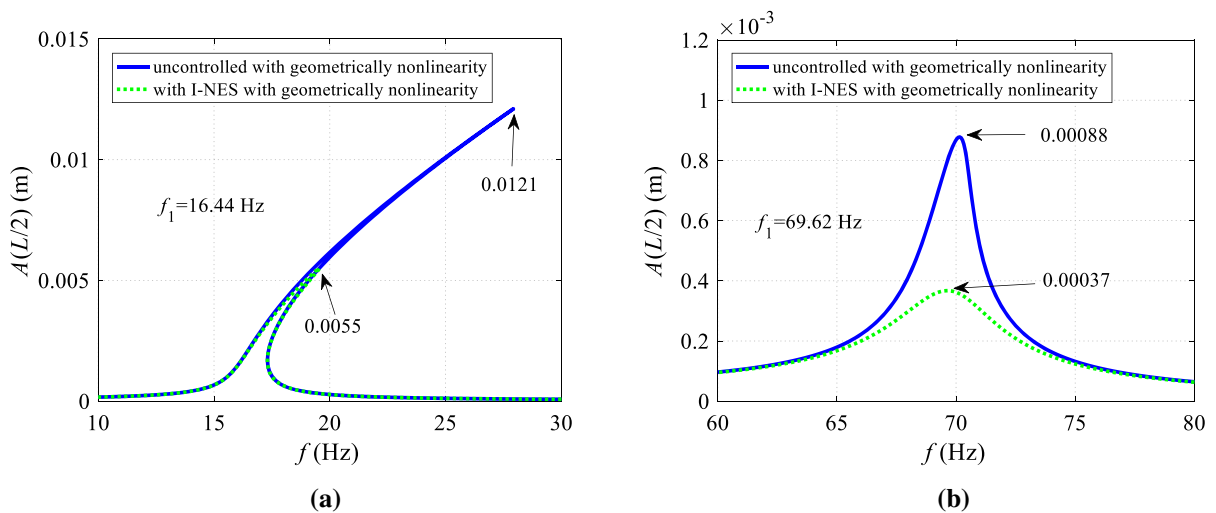


**Fig. 10** Vibration suppression analysis of I-NES at the midpoint of a geometrically nonlinear beam: **a** The first-order main resonance:  $f_1 = 16.44$  Hz; **b** The third-order main resonance:  $f_3 = 69.62$  Hz

of the beam is not considered, the vibration suppression percentage of the I-NESs is 58.43%. When considering the geometric nonlinearity of the beam, the vibration suppression percentage of the I-NESs is 58.18%. For the third-order main resonance at the midpoint of the beam, when the geometric nonlinearity of the beam is not considered, the vibration suppression percentage of the I-NESs is 58.41%. When the geometric nonlinearity of the beam is considered, the vibration suppression percentage of

the I-NESs is 58.16%. It can be seen that the I-NESs have a very good vibration suppression effect whether the geometric nonlinearity is considered or not. However, as shown in Figs. 7b, 8b, 9b, and 10b, for either the left boundary or the midpoint of the beam, compared with the first-order main resonance, the geometric nonlinearity of the third-order main resonance has little effect on the response of the beam.

**Table 3** Influence of I-NES on steady state amplitude frequency with or without geometric nonlinearity with  $U_0 = 0.0001$  m

Position	Main resonance	System	$A_u$ (m)	$A_c$ (m)	$R_A$ (%)
Left boundary	$f_1 = 16.44$ Hz	Linear	0.0082	0.0019	76.53
		Geometrically nonlinear	0.0049	0.0021	57.47
	$f_3 = 69.62$ Hz	Linear	0.0019	0.00077	58.43
		Geometrically nonlinear	0.0018	0.00077	58.18
Midpoint	$f_1 = 16.44$ Hz	Linear	0.0201	0.005	74.99
		Geometrically nonlinear	0.0121	0.0055	54.49
	$f_3 = 69.62$ Hz	Linear	0.00088	0.00037	58.41
		Geometrically nonlinear	0.00088	0.00037	58.16

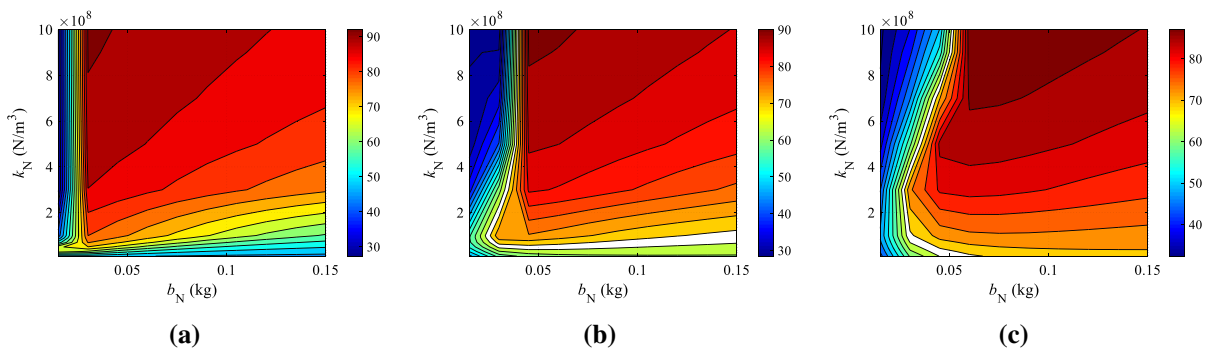


**Fig. 11** Two-dimensional contour maps near the optimum inertial mass at the left boundary of the beam: **a**  $c_N = 1$  N·s/m; **b**  $c_N = 2$  N·s/m; **c**  $c_N = 3$  N·s/m

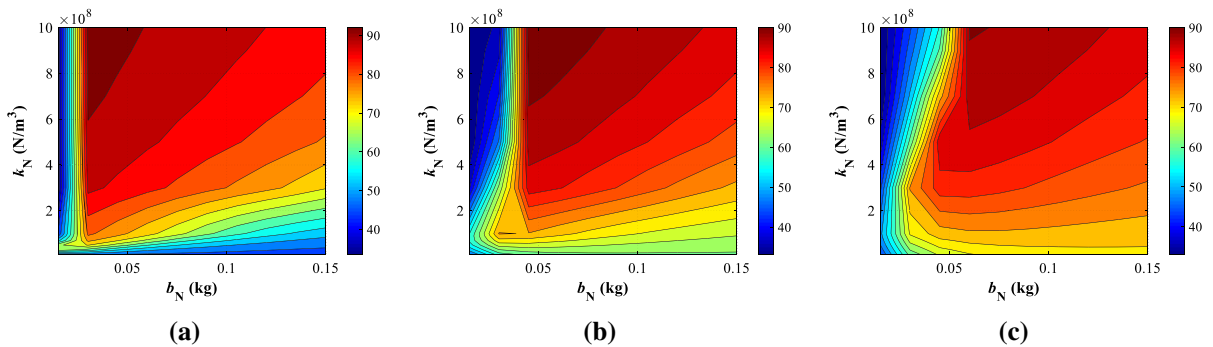


**Fig. 12** Two-dimensional contour maps near the optimum inertial mass at the midpoint of the beam: **a**  $c_N = 1$  N·s/m; **b**  $c_N = 2$  N·s/m; **c**  $c_N = 3$  N·s/m

**5 Parameter optimization of I-NES**

Since the amplitude of the first-order main resonance is larger than that of the third-order main resonance, only the first-order main resonance of the beam is considered in the following discussion of the parameter of the I-NESs. Taking the damping of the inertial

nonlinear energy sink as a fixed value, the influence of the change of inertial mass and cubic nonlinear stiffness on the damping effect of the inertial nonlinear energy sink is discussed.

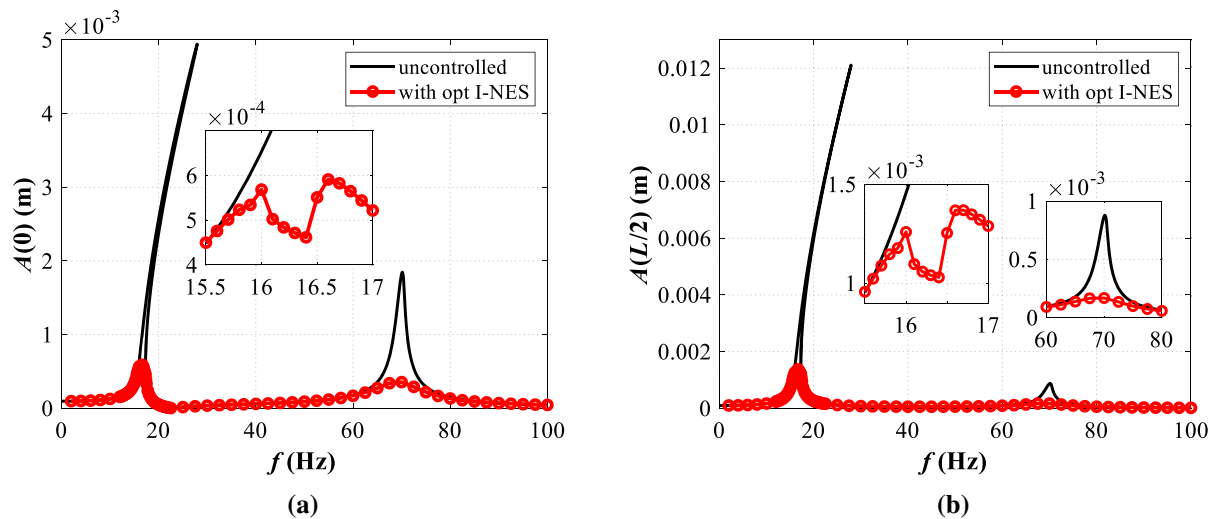


**Fig. 13** Vibration suppression effect of the optimal I-NES at damping: **a** The left boundary; **b** The midpoint

### 5.1 Optimal range of I-NES for different damping

For the damping  $c_N = 1, 2,$  and  $3$  N·s/m, when the damping and cubic nonlinearity change simultaneously, the two-dimensional contour maps near the optimal inertial mass at the left boundary and midpoint of the beam are shown in Figs. 11, 12.

The optimal parameters of the inertial nonlinear energy sink with different damping are shown in Table 4.

It can be concluded from Table 4 that the optimal parameters value of the inertial nonlinear energy sink for the left boundary and the midpoint are the same. Moreover, the variation trend if the vibration suppression effect of the inertial nonlinear energy sink on the left boundary and the midpoint with the parameters is also the same. As damping increases, the inertial mass coefficient to achieve the best vibration suppression effect gradually increases, while the vibration suppression effect is slightly reduced.

### 5.2 Analysis of the solution response for the optimal parameters

The optimization parameters of Fig. 11c are selected. For  $b_N = 0.06$  kg,  $c_N = 3$  N·s/m and  $k_N = 1 \times 10^9$  N/m<sup>3</sup>, the vibration suppression effect shown in Fig. 13. When considering geometric nonlinearity, it can be seen that the optimized I-NES also has a significant damping effect, and the first-order main resonance

**Table 4** The numerical value of inertial nonlinear energy sink for the optimal vibration-suppression effect for different damping

Position	$c_N$ (N·s/m)	$b_N$ (kg)	$k_N$ (N/m <sup>3</sup> )	$R_A$ (%)
Left boundary	1	0.03	$1 \times 10^9$	92.66
	2	0.045	$1 \times 10^9$	90.72
	3	0.06	$1 \times 10^9$	89.19
Midpoint	1	0.03	$1 \times 10^9$	93.8
	2	0.045	$1 \times 10^9$	91.86
	3	0.06	$1 \times 10^9$	90.27

vibration suppression effect reaches 90%. The third-order main resonance can also be well suppressed.

Based on the parameters in Fig. 13, the time history curves of the nonlinear beam with the optimized I-NESs for  $f = 16.6$  Hz are shown in Fig. 14. It can be seen that the response of the beam is strong quasi-periodic response. The response of the I-NES is strongly modulated response (SMR). This indicated that the I-NES is activated well.

## 6 Conclusions

This paper reports a study of the vibration response of an elastic beam system with I-NESs, in which the geometric nonlinear characteristic of the beam is

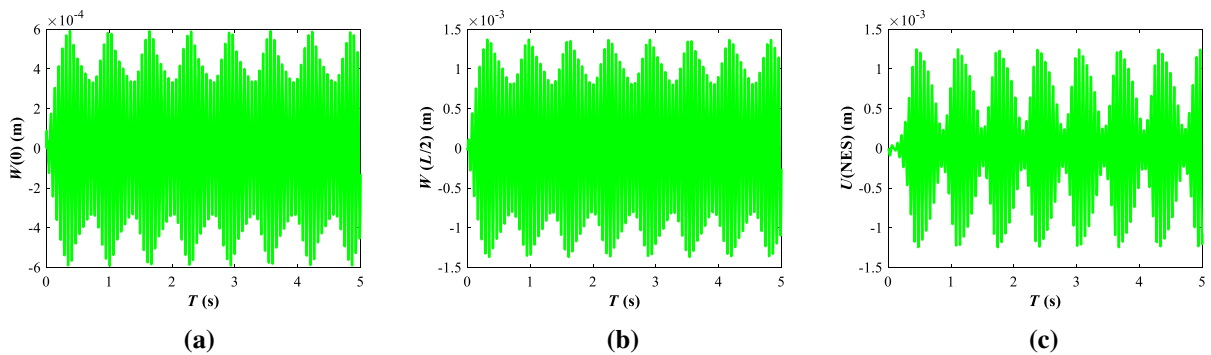


**Fig. 14** Time history of the nonlinear beam with the optimal I-NES for  $f = 16.6$  Hz: **a** The left boundary; **b** The midpoint; **c** The I-NES

considered. The partial differential equation of the system is discretized by the Galerkin method, and the steady amplitude-frequency response curve of the system is approximately solved based on the harmonic balance method, with numerical verification being carried out. By adjusting the inertial mass, damping parameters, and cubic nonlinear stiffness of the I-NESs, the influence of the change of the parameters on the vibration reduction effect of the system is analyzed, and the optimal range of parameters is discussed. Below are the specific conclusions.

When the geometric nonlinearity of the beam is considered, the I-NESs applied to the boundaries of an elastic beam can effectively suppress the transverse vibration of the beam. Comparison results show that for the first-order main resonance, the geometric nonlinearity of the beam strengthens its nonlinear hardening characteristics and reduces the vibration-suppression effect of the I-NES. Therefore, the geometric nonlinearity of the beam cannot be ignored in engineering research.

Here are the optimization results when considering geometric nonlinearity: The vibration reduction percentage of an optimized I-NES can be as high as 90%. In that case, the parameters of I-NES are  $b = 0.06$  kg,  $c_N = 3$  N-s/m and  $k_N = 1 \times 10^9$  N/m<sup>3</sup>. For the optimized I-NES, the time series response exhibit the strongly modulated response (SMR).

**Acknowledgements** The work presented in this paper was supported by the National Natural Science Foundation of China (12002217, 11902203, 12022213) and Liaoning Revitalization Talents Program (XLYC1807172).

**Funding** The authors have not disclosed any funding.

## Declarations

**Conflict of interest** The authors declare that they have no conflict of interest.

**Data availability** The raw/processed data required to reproduce these findings cannot be shared at this time as the data also forms part of an ongoing study.

## References

- Kerschen, G., Lee, Y.S., Vakakis, A.F., McFarland, D.M., Bergman, L.A.: Irreversible passive energy transfer in coupled oscillators with essential nonlinearity. *SIAM J. Appl. Math.* **66**, 648–679 (2006). <https://doi.org/10.1137/040613706>
- Gendelman, O., Manevitch, L.I., Vakakis, A.F., M'Closkey, R.: Energy pumping in nonlinear mechanical oscillators: part I—dynamics of the underlying hamiltonian systems. *J. Appl. Mech.* **68**, 34–41 (2001). <https://doi.org/10.1115/1.1345524>
- Blanchard, A., Bergman, L.A., Vakakis, A.F.: Vortex-induced vibration of a linearly sprung cylinder with an internal rotational nonlinear energy sink in turbulent flow. *Nonlinear Dyn.* **99**, 593–609 (2020). <https://doi.org/10.1007/s11071-019-04775-3>
- Viguié, R., Peeters, M., Kerschen, G., Golinval, J.C.: Energy transfer and dissipation in a duffing oscillator coupled to a nonlinear attachment. *J. Comput. Nonlinear Dyn.* **4**, 1–13 (2009). <https://doi.org/10.1115/1.3192130>
- Viguié, R., Kerschen, G.: Nonlinear vibration absorber coupled to a nonlinear primary system: a tuning methodology. *J. Sound Vib.* **326**, 780–793 (2009). <https://doi.org/10.1016/j.jsv.2009.05.023>
- Gourc, E., Michon, G., Seguy, S., Berlioz, A.: Experimental investigation and design optimization of targeted energy transfer under periodic forcing. *J. Vib. Acoust. Trans. ASME*. **136**, 1–8 (2014). <https://doi.org/10.1115/1.4026432>
- Ding, H., Chen, L.Q.: Designs, analysis, and applications of nonlinear energy sinks, (2020)
- Bergeot, B., Bellizzi, S., Cochelin, B.: Passive suppression of helicopter ground resonance instability by means of a

- strongly nonlinear absorber. *Adv. Aircr. Spacecr. Sci.* **3**, 271–298 (2016). <https://doi.org/10.12989/aas.2016.3.3.271>
9. Yang, K., Zhang, Y.W., Ding, H., Yang, T.Z., Li, Y., Chen, L.Q.: Nonlinear energy sink for whole-spacecraft vibration reduction. *J. Vib. Acoust. Trans. ASME*. (2017). <https://doi.org/10.1115/1.4035377>
  10. Wang, J., Li, H., Wang, B., Liu, Z., Zhang, C.: Development of a two-phased nonlinear mass damper for displacement mitigation in base-isolated structures. *Soil Dyn. Earthq. Eng.* **123**, 435–448 (2019). <https://doi.org/10.1016/j.soildyn.2019.05.007>
  11. Lu, X., Liu, Z., Lu, Z.: Optimization design and experimental verification of track nonlinear energy sink for vibration control under seismic excitation. *Struct. Control Heal. Monit.* **24**, e2033 (2017). <https://doi.org/10.1002/stc.2033>
  12. Chen, L.Q., Li, X., Lu, Z.Q., Zhang, Y.W., Ding, H.: Dynamic effects of weights on vibration reduction by a nonlinear energy sink moving vertically. *J. Sound Vib.* **451**, 99–119 (2019). <https://doi.org/10.1016/j.jsv.2019.03.005>
  13. Xue, J.-R., Zhang, Y.-W., Ding, H., Chen, L.-Q.: Vibration reduction evaluation of a linear system with a nonlinear energy sink under a harmonic and random excitation. *Appl. Math. Mech.* **41**, 1–14 (2020). <https://doi.org/10.1007/s10483-020-2560-6>
  14. Zhang, Y., Xu, K., Zang, J., Ni, Z., Zhu, Y., Chen, L.: Dynamic design of a nonlinear energy sink with NiTiNOL-steel wire ropes based on nonlinear output frequency response functions. *Appl. Math. Mech.* **40**, 1791–1804 (2019). <https://doi.org/10.1007/s10483-019-2548-9>
  15. Lu, Z., Wang, Z., Zhou, Y., Lu, X.: Nonlinear dissipative devices in structural vibration control: a review. *J. Sound Vib.* **423**, 18–49 (2018). <https://doi.org/10.1016/j.jsv.2018.02.052>
  16. Bitar, D., Ture Savadkoobi, A., Lamarque, C.H., Gourdon, E., Collet, M.: Extended complexification method to study nonlinear passive control. *Nonlinear Dyn.* **99**, 1433–1450 (2020). <https://doi.org/10.1007/s11071-019-05365-z>
  17. AL-Shudeifat, M.A.: Nonlinear energy sinks with nontraditional kinds of nonlinear restoring forces. *J. Vib. Acoust.* **139**, 1–5 (2017). <https://doi.org/10.1115/1.4035479>
  18. AL-Shudeifat, M.A., Wierschem, N.E., Bergman, L.A., Vakakis, A.F.: Numerical and experimental investigations of a rotating nonlinear energy sink. *Meccanica* **52**, 763–779 (2017). <https://doi.org/10.1007/s11012-016-0422-2>
  19. Farid, M., Gendelman, O.V.: Tuned pendulum as nonlinear energy sink for broad energy range. *J. Vib. Control.* **23**, 373–388 (2017). <https://doi.org/10.1177/1077546315578561>
  20. Tsiatas, G.C., Charalampakis, A.E.: A new hysteretic nonlinear energy sink (HNES). *Commun. Nonlinear Sci. Numer. Simul.* **60**, 1–11 (2018). <https://doi.org/10.1016/j.cnsns.2017.12.014>
  21. Habib, G., Romeo, F.: The tuned bistable nonlinear energy sink. *Nonlinear Dyn.* **89**, 179–196 (2017). <https://doi.org/10.1007/s11071-017-3444-y>
  22. Farid, M., Gendelman, O.V., Babitsky, V.I.: Dynamics of a hybrid vibro-impact nonlinear energy sink. *ZAMM J. Appl. Math. Mech./Zeitschrift für Angew. Math. Und. Mech.* (2019). <https://doi.org/10.1002/zamm.201800341>
  23. Zang, J., Cao, R.-Q., Zhang, Y.-W., Fang, B., Chen, L.-Q.: A lever-enhanced nonlinear energy sink absorber harvesting vibratory energy via giant magnetostrictive-piezoelectricity. *Commun. Nonlinear Sci. Numer. Simul.* **95**, 105620 (2021). <https://doi.org/10.1016/J.CNSNS.2020.105620>
  24. Smith, M.C.: Synthesis of mechanical networks: the inerter'. (2002)
  25. Papageorgiou, C., Houghton, N.E., Smith, M.C.: Experimental testing and analysis of inerter devices. *J. Dyn. Syst. Meas. Control.* **131**, 1–11 (2009). <https://doi.org/10.1115/1.3023120>
  26. Shi, X., Zhu, S.: Dynamic characteristics of stay cables with inerter dampers. *J. Sound Vib.* **423**, 287–305 (2018). <https://doi.org/10.1016/j.jsv.2018.02.042>
  27. Zhang, Y.W., Lu, Y.N., Zhang, W., Teng, Y.Y., Yang, H.X., Yang, T.Z., Chen, L.Q.: Nonlinear energy sink with inerter. *Mech. Syst. Signal Process.* **125**, 52–64 (2019). <https://doi.org/10.1016/j.ymsp.2018.08.026>
  28. Zhang, Z., Lu, Z.Q., Ding, H., Chen, L.Q.: An inertial nonlinear energy sink. *J. Sound Vib.* **450**, 199–213 (2019). <https://doi.org/10.1016/j.jsv.2019.03.014>
  29. Yang, T.Z., Yang, X.D., Li, Y., Fang, B.: Passive and adaptive vibration suppression of pipes conveying fluid with variable velocity. *JVC/J. Vib. Control.* **20**, 1293–1300 (2014). <https://doi.org/10.1177/1077546313480547>
  30. Mamaghani, A.E., Khadem, S.E., Bab, S.: Vibration control of a pipe conveying fluid under external periodic excitation using a nonlinear energy sink. *Nonlinear Dyn.* **86**, 1761–1795 (2016). <https://doi.org/10.1007/s11071-016-2992-x>
  31. Geng, X., Ding, H., Wei, K., Chen, L.: Suppression of multiple modal resonances of a cantilever beam by an impact damper. *Appl. Math. Mech.* **41**, 383–400 (2020). <https://doi.org/10.1007/s10483-020-2588-9>
  32. Ding, H., Yang, Y., Chen, L.Q., Yang, S.P.: Vibration of vehicle-pavement coupled system based on a Timoshenko beam on a nonlinear foundation. *J. Sound Vib.* **333**, 6623–6636 (2014). <https://doi.org/10.1016/j.jsv.2014.07.016>
  33. Ding, H., Huang, L., Mao, X., Chen, L.: Primary resonance of traveling viscoelastic beam under internal resonance. *Appl. Math. Mech.* (2017). <https://doi.org/10.1007/s10483-016-2152-6>
  34. Ding, H., Lu, Z.Q., Chen, L.Q.: Nonlinear isolation of transverse vibration of pre-pressure beams. *J. Sound Vib.* **442**, 738–751 (2019). <https://doi.org/10.1016/j.jsv.2018.11.028>
  35. Chouvion, B.: A wave approach to show the existence of detached resonant curves in the frequency response of a beam with an attached nonlinear energy sink. *Mech. Res. Commun.* **95**, 16–22 (2019). <https://doi.org/10.1016/j.mechrescom.2018.11.006>
  36. Zang, J., Zhang, Y.W., Ding, H., Yang, T.Z., Chen, L.Q.: The evaluation of a nonlinear energy sink absorber based on the transmissibility. *Mech. Syst. Signal Process.* **125**, 99–122 (2019). <https://doi.org/10.1016/j.ymsp.2018.05.061>
  37. Lu, Z., Li, K., Ding, H., Chen, L.: Nonlinear energy harvesting based on a modified snap-through mechanism. *Appl. Math. Mech.* **40**, 167–180 (2019). <https://doi.org/10.1007/s10483-019-2408-9>



38. Vakakis, A.F.: Passive nonlinear targeted energy transfer. *Phil. Trans. R. Soc. A.* (2018). <https://doi.org/10.1098/rsta.2017.0132>
39. Li, X., Zhang, Y., Ding, H., Chen, L.: Integration of a nonlinear energy sink and a piezoelectric energy harvester. *Appl. Math. Mech.* **38**, 1019–1030 (2017). <https://doi.org/10.1007/s10483-017-2220-6>
40. Parseh, M., Dardel, M., Ghasemi, M.H.: Investigating the robustness of nonlinear energy sink in steady state dynamics of linear beams with different boundary conditions. *Commun. Nonlinear Sci. Numer. Simul.* **29**, 50–71 (2015). <https://doi.org/10.1016/j.cnsns.2015.04.020>
41. Yang, Y., Wang, X.: Investigation into the linear velocity response of cantilever beam embedded with impact damper. *JVC/J. Vib. Control.* **25**, 1365–1378 (2019). <https://doi.org/10.1177/1077546318821711>
42. Zhang, Y.W., Hou, S., Zhang, Z., Zang, J., Ni, Z.Y., Teng, Y.Y., Chen, L.Q.: Nonlinear vibration absorption of laminated composite beams in complex environment. *Nonlinear Dyn.* **99**, 2605–2622 (2020). <https://doi.org/10.1007/s11071-019-05442-3>
43. Zhang, T., Ouyang, H., Zhang, Y.O., Lv, B.L.: Nonlinear dynamics of straight fluid-conveying pipes with general boundary conditions and additional springs and masses. *Appl. Math. Model.* **40**, 7880–7900 (2016). <https://doi.org/10.1016/j.apm.2016.03.050>
44. Li, Y.X., Sun, L.Z.: Transverse vibration of an undamped elastically connected double-beam system with arbitrary boundary conditions. *J. Eng. Mech.* (2015). [https://doi.org/10.1061/\(ASCE\)EM.1943-7889](https://doi.org/10.1061/(ASCE)EM.1943-7889)
45. Ding, H., Zhu, M., Chen, L.: Dynamic stiffness method for free vibration of an axially moving beam with generalized boundary conditions. *Appl. Math. Mech.* **40**, 911–924 (2019). <https://doi.org/10.1007/s10483-019-2493-8>
46. Wang, Y.R., Fang, Z.W.: Vibrations in an elastic beam with nonlinear supports at both ends. *J. Appl. Mech. Tech. Phys.* **56**, 337–346 (2015). <https://doi.org/10.1134/S0021894415020200>
47. Zang, J., Cao, R.-Q., Zhang, Y.-W.: Steady-state response of a viscoelastic beam with asymmetric elastic supports coupled to a lever-type nonlinear energy sink. *Nonlinear Dyn.* (2021). <https://doi.org/10.1007/s11071-021-06625-7>
48. Zhang, Z., Ding, H., Zhang, Y.W., Chen, L.Q.: Vibration suppression of an elastic beam with boundary inerter-enhanced nonlinear energy sinks. *Acta Mech. Sin.* (2021). <https://doi.org/10.1007/s10409-021-01062-6>
49. Ding, H., Zhu, M.H., Chen, L.Q.: Nonlinear vibration isolation of a viscoelastic beam. *Nonlinear Dyn.* **92**, 325–349 (2018). <https://doi.org/10.1007/s11071-018-4058-8>
50. Ding, H., Li, Y., Chen, L.Q.: Nonlinear vibration of a beam with asymmetric elastic supports. *Nonlinear Dyn.* **95**, 2543–2554 (2019). <https://doi.org/10.1007/s11071-018-4705-0>
51. Ding, H., Dowell, E.H., Chen, L.Q.: Transmissibility of bending vibration of an elastic beam. *J. Vib. Acoust. Trans. ASME.* (2018). <https://doi.org/10.1115/1.4038733>
52. Mao, X.Y., Ding, H., Chen, L.Q.: Vibration of flexible structures under nonlinear boundary conditions. *J. Appl. Mech. Trans. ASME.* (2017). <https://doi.org/10.1115/1.4037883>
53. Mao, X.Y., Ding, H., Chen, L.Q.: Passive isolation by nonlinear boundaries for flexible structures. *J. Vib. Acoust. Trans. ASME.* (2019). <https://doi.org/10.1115/1.4042932>

**Publisher's Note** Springer Nature remains neutral with regard to jurisdictional claims in published maps and institutional affiliations.